Influence of Sulfur Oxidation State and Substituents on Sulfur-Bridged Luminescent Copper(I) Complexes Showing Thermally Activated Delayed Fluorescence

Christopher M. Brown,[‡] Chenfei Li,[§] Veronica Carta,[‡] Wenbo Li,[¶] Zhen Xu,[‡] Pedro Henrique Fazza Stroppa,[§] Ifor D. W. Samuel,[¶] Eli Zysman-Colman[§] and Michael O. Wolf*[‡]

[‡] *Department of Chemistry, University of British Columbia, Vancouver, BC, V6T 1Z1, Canada*

[§] *Organic Semiconductor Centre, EaStCHEM School of Chemistry, University of St. Andrews, St. Andrews, Fife, KY16 9ST, UK*

[¶] *Organic Semiconductor Centre, SUPA School of Physics and Astronomy, University of St. Andrews, Fife, KY16 9SS, UK*

ABSTRACT

Copper(I) complexes are seen as more sustainable alternatives to those containing metal ions such as iridium and platinum for emitting devices. Copper(I) complexes have the ability to radiatively decay via a thermally activated delayed fluorescence (TADF) pathway, leading to higher photoluminescent quantum yields. In this work we discuss six new heteroleptic Cu(I) complexes of the diphosphine–diimine motif. The diphosphine ligands employed are (oxydi-2,1-phenylene)bis(diphenylphosphine) (DPEPhos) and the diimine fragments are sulfur-bridged dipyridyl ligands (DPS) which are functionalized at the 6,6′-positions of the pyridyl rings (R = H, Me, Ph), and have varying oxidation states at the bridging sulfur atom (S, SO_2). The proton (**Cu-DPS**, **Cu-DPSO$_2$**) and phenyl (**Cu-Ph-DPS**, **Cu-Ph-DPSO$_2$**) substituted species are found to form monometallic complexes, while those with methyl substitution (**Cu-**

Me-DPS, **Cu-Me-DPSO$_2$**) are found to have a "Goldilocks" degree of steric bulk leading to bimetallic species. All six Cu(I) complexes show emission in the solid state, with the photophysical properties characterized by low temperature steady-state and time-resolved spectroscopies and variable temperature time-correlated single photon counting (TCSPC). **Cu-DPS**, **Cu-DPSO$_2$**, **Cu-Me-DPS**, **Cu-Me-DPSO$_2$** and **Cu-Ph-DPSO$_2$** were shown to emit via a TADF mechanism, while **Cu-Ph-DPS** showed photoluminescence properties consistent with triplet ligand-centered (^{3}LC) emission.

INTRODUCTION

Luminescent materials based on transition metal complexes have long inspired substantial research efforts due to their ability to be implemented in a range of technologies. These include solar applications,[1] photocatalysis[2] and, in particular, lighting technologies such as organic light-emitting diodes (OLEDs)[3-5] or light-emitting electrochemical cells (LEECs).[6,7] Often these lighting applications are dominated by the use of third-row transition metals such as Ir,[8,9] and Pt[10] due to their high degrees of color tuneability, efficiencies and stabilities. These metals, however, are limited by their very low abundances in the Earth's crust, and as such efforts are required to find more sustainable alternatives. In particular, coinage metals with a d^{10} configuration such as Cu(I), Ag(I) and Au(I) are promising candidates due to their higher abundance in the Earth's crust and the absence of accessible metal-centered (MC) states that serve as non-radiative and decomposition pathways in most other metal complexes. Copper(I) species, especially, have attracted considerable interest from the research community in the past decade.[3,11-14]

Emissive copper(I) complexes have been shown to adopt a number of structures. These range from homo- or heteroleptic mononuclear species containing diimine (N^N), diphosphine (P^P) or imine-phosphine (N^P) ligands,[15-18] to polynuclear species that can be bridged by the

aforementioned ligands[19] or halide atoms,[20] to tetranuclear cubane structures.[21] The geometry about the copper center can range from linear,[22-24] to trigonal planar,[25-30] to tetrahedral.[31-38] The ability for copper(I) to adopt a variety of structures allows for an array of different photophysical properties, which have been extensively studied in solution, in the solid state as powders, crystals and in polymer and small molecule host matrices.

In ground-state tetracoordinate Cu(I) complexes, the metal center has a d^{10} configuration adopting a pseudotetrahedral (D_{2d}) geometry, which upon photoexcitation usually undergoes a metal-to-ligand charge transfer (MLCT), formally oxidizing the metal center to a d^9 Cu(II) configuration. Once in this excited-state, the complex undergoes a fast (<1 ps) Jahn-Teller distortion to a more flattened geometry, opening up nonradiative decay pathways such as exciplex formation with coordinating species.[39,40] This distorted geometry is preserved until relaxation to the ground state occurs. Rational design of the ligands has been shown to inhibit this distortion through structural modification aimed at introducing constraints to maintain the tetrahedral geometry, thereby increasing the lifetime of the excited state and the photoluminescence quantum efficiency of the complex.[41] Emission of Cu(I) species can occur via two competitive routes: thermally activated delayed fluorescence (TADF), and phosphorescence, where one or both pathways can be operational. In TADF, otherwise non-emissive triplet states can be upconverted to singlet states, frequently resulting in higher photoluminescence quantum yields.[3] As a function of the small exchange energy resulting from the MLCT excited state, there is a very small singlet-triplet energy gap, ΔE_{ST}, that permits thermally activated reverse intersystem crossing (rISC) at ambient temperature.

Our group has shown that varying the oxidation state at sulfur can have pronounced effects on the electronic properties of organic chromophores[42,43] and luminescent inorganic complexes. [44-46] In this study, the synthesis and optoelectronic characterization of a series of six new heteroleptic Cu(I) species utilizing sulfur-bridged dipyridyl ligands in either the sulfide

(II) or sulfone (VI) oxidation state as the N^N component, and bis[2-(diphenylphosphino)-phenyl]ether (DPEPhos) as the P^P component are discussed. We show that modulation of the sterics at the 6- and 6'-positions of the N^N ligand in conjunction with changes in the sulfur oxidation state influences the formation of mono or bimetallic species, and results in unexpected binding modes at the dipyridyl ligand with bonding observed through nitrogen, sulfur or oxygen atoms.

RESULTS AND DISCUSSION

Ligand Synthesis and Characterization

The sulfide-bridged compounds **DPS**, **Me-DPS** and **Ph-DPS** were synthesized *via* nucleophilic aromatic substitution of thiourea with 2-bromopyridine, 2-bromo-6-methylpyridine or 2-bromo-6-phenylpyridine, respectively (Scheme 1). The desired sulfone species, **$DPSO_2$**, **Me-$DPSO_2$** and **Ph-$DPSO_2$** were obtained through oxidation of the appropriate dipyridyl sulfide pro-ligand with 30% H_2O_2 using a niobium carbide (NbC) catalyst. High yields were attained, and the six pro-ligands were characterized using NMR spectroscopy, high resolution mass spectrometry and infrared spectroscopy. ^{1}H and ^{13}C signals were assigned using COSY, HSQC and HMBC experiments (Figures S1–S20).

Scheme 1. Synthesis of (a) pro-ligands and (b) Cu(I) complexes discussed in this work.

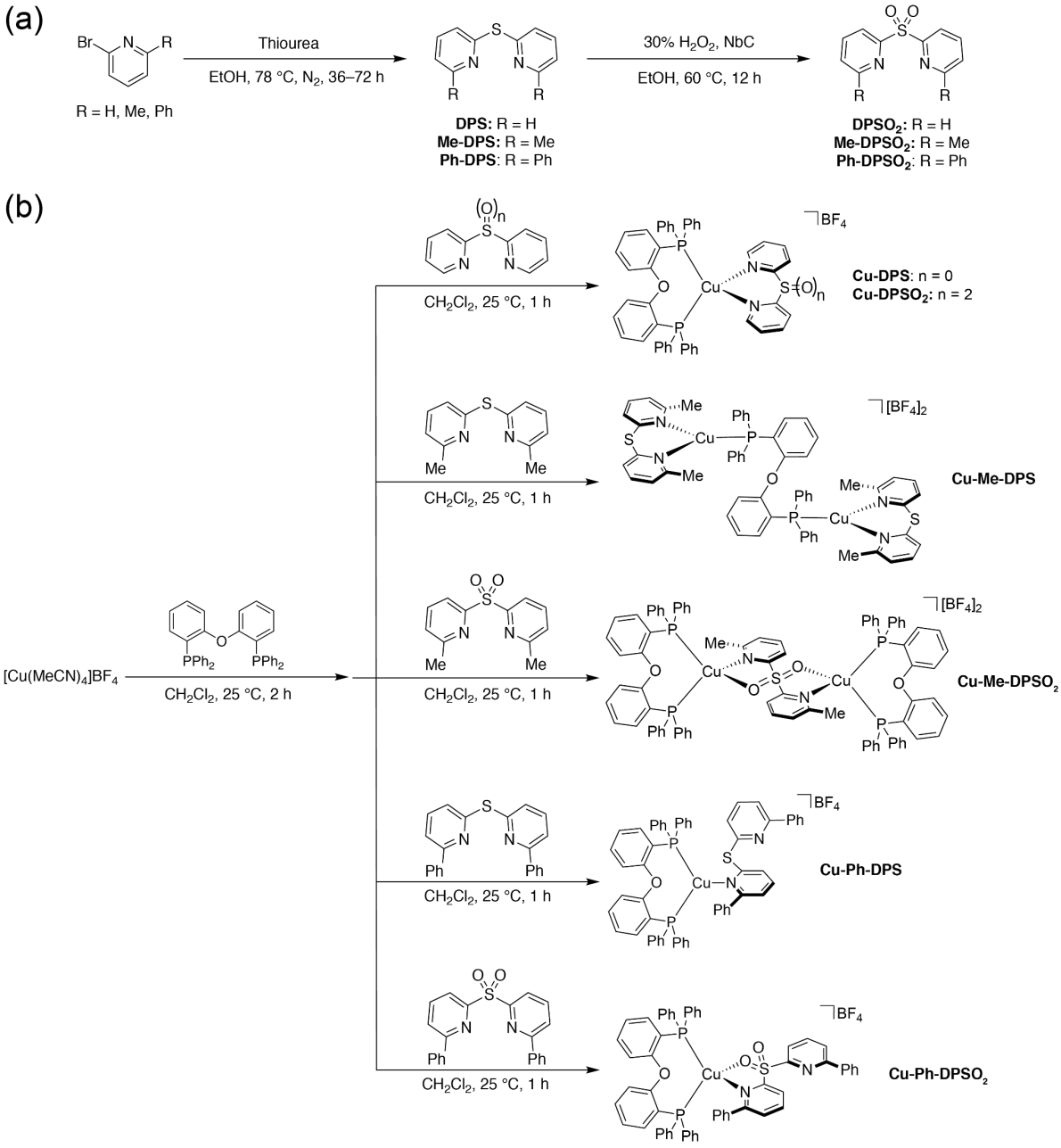

Synthesis and Characterization of Cu(I) Complexes

The six copper(I) complexes were prepared using synthetic methods described in the literature[47] and shown in Scheme 1. To a stirring solution of $[Cu(MeCN)_4][BF_4]$ in CH_2Cl_2 at 25 ˚C was added the desired molar ratio of DPEPhos followed by the desired molar ratio of the N^N pro-ligand (N^N = **DPS**, **DPSO$_2$**, **Me-DPS**, **Me-DPSO$_2$**, **Ph-DPS** or **Ph-DPSO$_2$**).

Following addition of Et_2O to promote precipitation from solution, the species were all isolated in high yields as off-white to yellow powders that required no further purification. ^{1}H, ^{13}C and ^{31}P NMR spectra were collected and resonances assigned using COSY, HSQC and HMBC experiments, with the broad ^{31}P signals that are observed attributed to quadrupole coupling with the copper atom. Complexes **Cu-DPS**, **Cu-DPSO$_2$**, **Cu-Ph-DPS** and **Cu-Ph-DPSO$_2$** were synthesized using equimolar ratios of $[Cu(MeCN)_4][BF_4]$, DPEPhos and the appropriate diimine ligand and isolated as monometallic species. HR-ESI mass spectra show a product peak corresponding to $[M–BF_4]^+$ and exhibit a characteristic copper isotope pattern. NMR experiments show **Cu-DPS**, **Cu-DPSO$_2$** and **Cu-Ph-DPS** are coordinated by the diimine in an *N*,*N* binding motif (Figures S21–S27, S28–S34 and S50–S56, respectively), and *N*,*O* binding seen in **Cu-Ph-DPSO$_2$** (Figures S57–S62), with all six complexes tetrahedral about the copper center in solution.

Interestingly, for species containing methyl groups in the 6- and 6'-positions of the dipyridyl ligand (**Me-DPS** and **Me-DPSO$_2$**) bimetallic complexes **Cu-Me-DPS** and **Cu-Me-DPSO$_2$** were isolated where the DPEPhos ligand adopts an unusual bridging mode (Scheme 1). While the analogous complex $[Cu(DPEPhos)(tmbpy)][BF_4]$ (tmbpy = 4,4',6,6'-tetramethyl-2,2′-bipyridine) is monometallic,[34] the larger bite angle afforded by the addition of a sulfur atom between the two pyridyl rings coupled with the added bulk of the methyl substituents presumably causes the steric constraints to be too great to form the typical $[Cu(N\text{^}N)(P\text{^}P)]^+$ four-coordinate species. NMR experiments with **Cu-Me-DPS** show a bimetallic complex with each discrete Cu(I) complexed with the **Me-DPS** ligand and the two metal centers bridged by the DPEPhos ligand (Figures S35–S41). This bridged binding mode for the DPEPhos ligand has not been reported, with previous examples containing halide bridges in tandem with DPEPhos.[48,49] The ^{1}H NMR spectrum of **Cu-Me-DPS** shows sharp signals for the DPEPhos ligand, but broad signals attributed to the **Me-DPS** ligand, likely caused by fluxional behavior

of this ligand on the NMR timescale. Low-temperature NMR experiments did not reveal a defined structure. **Cu-Me-DPSO$_2$** was likewise found to exist as a bimetallic species; however, instead of DPEPhos acting as a bridging ligand, **Me-DPSO$_2$** bridges the two copper(I) atoms with each discrete metal center bound in a *N,O* fashion through one pyridyl ring and one of the sulfone oxygen atoms (Figures S43–S49). Four-coordinate geometry about each Cu(I) is completed by a DPEPhos ligand. Syntheses of **Cu-Me-DPS** and **Cu-Me-DPSO$_2$** were also conducted using equimolar equivalents of [Cu(MeCN)$_4$][BF$_4$], DPEPhos and diimine ligands, and under these conditions the bridged, bimetallic structures still preferentially formed.

Single Crystal X-ray Diffraction

Single crystals of **Cu-DPS**, **Cu-DPSO$_2$**, **Cu-Me-DPS**, **Cu-Me-DPSO$_2$**, **Cu-Ph-DPS** and **Cu-Ph-DPSO$_2$** were grown by vapor diffusion of Et_2O into CH_2Cl_2 solutions of the complexes. Steric factors strongly affect the coordination chemistry of copper(I) when complexed with DPEPhos ligands. DPEPhos is a bulky, wide bite-angle bidentate ligand and it has been shown that when two DPEPhos ligands coordinate to copper(I), the metal adopts a trigonal geometry to reduce steric hindrance.[50] In [Cu(DPEPhos)$_2$][BF$_4$],only one DPEPhos is able to behave as a chelating unit while the second ligand binds through one phosphorus atom forming a trigonal species;[50] generally, copper(I) forms tetrahedral complexes in less sterically hindered systems.[51-53]

The six aforementioned copper(I) complexes were structurally characterized (Figure 1), with the data corroborating the geometries of the complexes inferred from the NMR spectra for all complexes except **Cu-Ph-DPS**. The six dipyridyl ligands each differ in both steric bulk and binding modes. **DPS**, **Me-DPS** and **Ph-DPS** act as bidentate ligands that coordinate to copper through both pyridyl nitrogen atoms, with **Me-DPS** and **Ph-DPS** possessing increasing

steric bulk due to the presence of methyl and phenyl groups in the 6- and 6'-positions. **DPSO$_2$**, **Me-DPSO$_2$** and **Ph-DPSO$_2$** each have two different binding modes, either through the pyridyl nitrogen atoms (*N*,*N*), or through one nitrogen and one sulfone oxygen (*N*,*O*). These ligands can therefore adopt a preferential coordination mode in order to reduce steric tension within the complex. The result is that with methyl groups present the complexes crystallize as bimetallic species where either DPEPhos or **Me-DPSO$_2$** bridge two copper atoms.

Cu-DPS (Figure 1(a)) and **Cu-DPSO$_2$** (Figure 1(c)) both crystallize as mononuclear complexes with the copper center presenting a distorted tetrahedral geometry coordinated to two dipyridyl ligand binding in an *N*,*N* mode. **Cu-Me-DPS** (Figure 1(b)) crystallizes as a dinuclear assembly in which the DPEPhos ligand bridges two copper atoms with a distorted trigonal geometry. **Cu-Me-DPSO$_2$** (Figure 1(d)) also crystallizes as a bimetallic complex, but with a coordination sphere about each copper atom that is distinct from **Cu-Me-DPS**. In this case the Cu(I) atoms have tetrahedral geometry with the bridging ligand **Me-DPSO$_2$** ligand binding in an *N*,*O* coordination mode to each of the two metal centers.

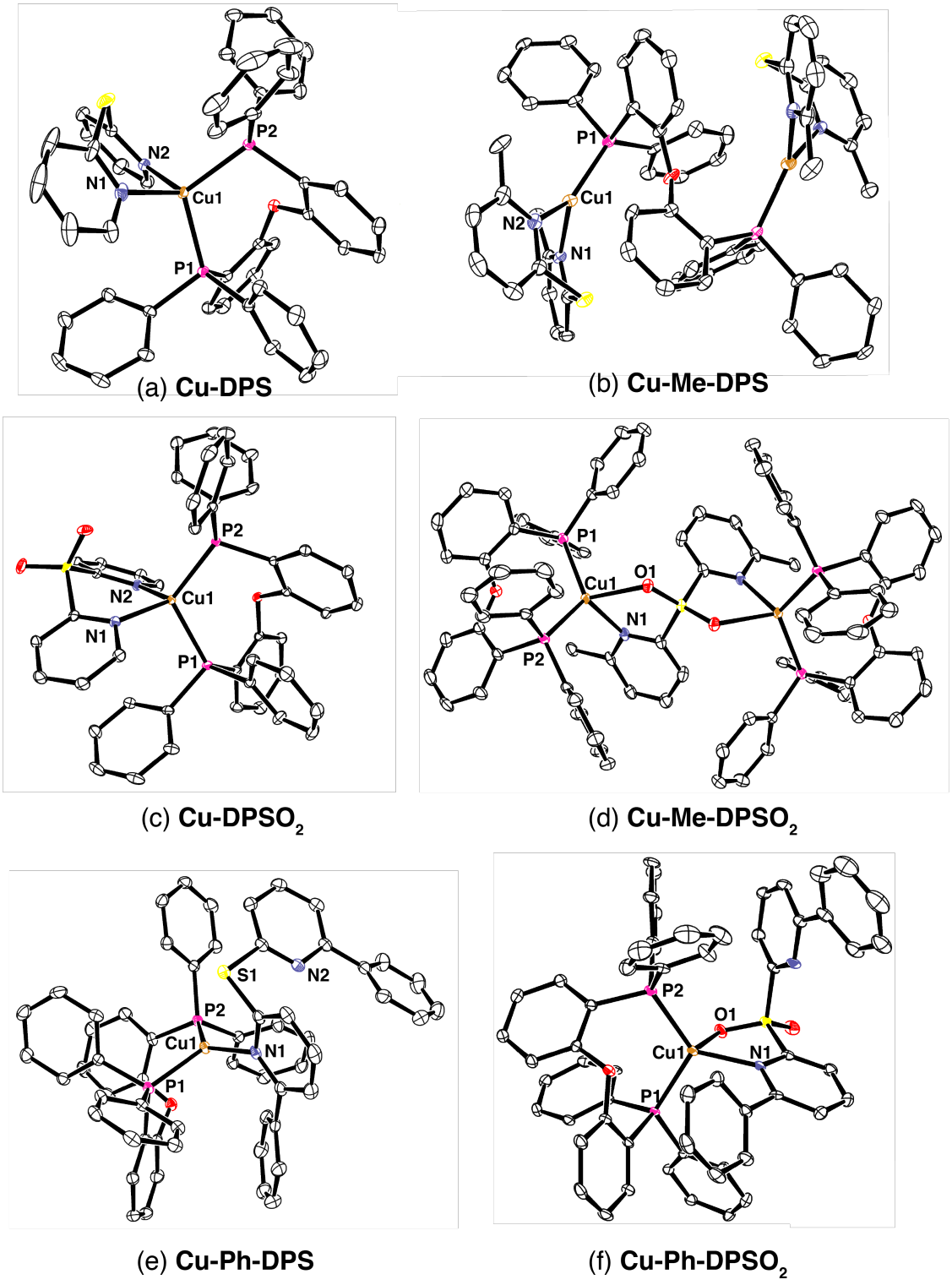

Figure 1. ORTEP representations of single crystal structures of (a) **Cu-DPS**; (b) **Cu-Me-DPS**; (c) **Cu-DPSO₂**; (d) **Cu-Me-DPSO₂**; (e) **Cu-Ph-DPS**; (f) **Cu-Ph-DPSO₂**. Ellipsoids are plotted at the 50% probability level. Hydrogen atoms, solvent molecules and $[BF_4]^-$ counter ions are removed for clarity.

As a consequence of the larger phenyl groups in **Ph-DPS** and **Ph-DPSO$_2$**, when these ligands are coordinated to copper in **Cu-Ph-DPS** and **Cu-Ph-DPSO$_2$**, they arrange in a structure with the two bulky phenyl groups pointing away from each other, thereby preventing the *N*,*N* coordination mode. However, despite the imposition of increased steric bulk, these species do not form bimetallic assemblies (as in **Cu-Me-DPS** and **Cu-Me-DPSO$_2$**) but monometallic species instead. In **Cu-Ph-DPS** (Figure 1(e)) the diimine ligand coordinates in a monodentate fashion via one of the two pyridyl nitrogen atoms and the resulting copper complex has a distorted trigonal geometry, differing from the four-coordinate species observed in solution. **Cu-Ph-DPSO$_2$** (Figure 1(f)) is coordinated with a *N*,*O* binding mode, but the diimine ligand does not bridge two copper atoms, as was observed with **Cu-Me-DPSO$_2$**. In both cases the DPEPhos ligand coordinates to one copper atom with a *P*,*P* binding mode.

Selected bond lengths and angles for the six complexes are reported in Table S1. All the complexes exhibit a distorted geometry. This is not surprising because the bite angle of the **DPS** and **DPSO$_2$** ligands are smaller than that of DPEPhos due to the size of the diphosphine chelate, and as a result the N–Cu–N bite angle is smaller than the P–Cu–P bite angle. Structural studies show that in all the tetrahedral complexes the P–Cu–P bite angles are in the range of 113–117º and the N–Cu–N bite angles are in the range of 93–97º, which is in agreement with literature reports for analogous structures.[19,50,53] The N–Cu–O angles in **Cu-Me-DPSO$_2$** and **Cu-Ph-DPSO$_2$** are smaller than expected for a tetrahedral complex at ~79º and 80º, respectively. The trigonal complexes have a distorted structure as well. A N–Cu–N angle of 96º and a P–Cu–N angle of 129º are seen in **Cu-Me-DPS**. In **Cu-Ph-DPS**, N–Cu–P angles are 110º and 135º, and the P–Cu–P angle is 114º. The distance between the copper center and the sulfur atom in **Cu-Ph-DPS** is quite long (2.9 Å), but similar copper-sulfur distances have been reported for other copper complexes.[54] However, the small S–Cu–N angle (63º) and the fact that the two phosphorus and the nitrogen atoms are almost coplanar, suggests that the structure

has a distorted trigonal planar geometry rather than a distorted tetrahedral geometry. The Cu–P and Cu–N bond lengths are all similar within the series reported here and to other mononuclear copper(I) complexes in the literature.[19] However, the Cu–O bond in **Cu-Me-DPSO$_2$** and in **Cu-Ph-DPSO$_2$** is quite long (2.4 Å), probably due to steric repulsion of the methyl and phenyl substituents and the DPEPhos phenyl groups.

Electrochemical Properties

The electrochemical behavior of the Cu(I) complexes was investigated using cyclic voltammetry (CV) of CH_2Cl_2 solutions *vs*. Fc/Fc^+ and referenced to SCE, with data summarized in Table 1 and CVs displayed in Figures S63–S64. All species display irreversible redox waves, with no change in the reversibility observed in scanning up to 1 Vs^{-1}. Two oxidation features are observed for each complex, with the first attributed to the Cu^+/Cu^{2+} oxidation.[51] In the unsubstituted species, an increase in oxidation potential is seen (1.03 V to 1.17 V) on oxidizing **Cu-DPS** to **Cu-DPSO$_2$** owing to the electron-withdrawing effect of the sulfone-bridged ligand on the coordinating nitrogen atoms. These potentials are significantly more positive than those seen for the reference complex [Cu(DPEPhos)(bpy)][PF_6], (E_{ox} = 0.72 V).[55]

Table 1. Electrochemical data of Cu(I) complexes in CH_2Cl_2 solutions.

	$E_{(ox)}$ (V) [a]	$E_{(red)}$ (V) [a]	E_{HOMO} (eV) [b]	E_{LUMO} (eV) [b]	ΔE_{redox} (V)
Cu-DPS	1.03	–0.93	–5.67	–3.71	1.96
	1.64				
Cu-DPSO$_2$	1.17	–1.01	–5.81	–3.63	2.18
	1.74				
Cu-Me-DPS	1.08	–1.01	–5.72	–3.63	2.09

	1.67				
Cu-Me-DPSO$_2$	1.13	–0.99	–5.77	–3.65	2.12
	1.73				
Cu-Ph-DPS	1.36	–0.85	–6.00	–3.79	2.21
Cu-Ph-DPSO$_2$	1.18	–1.01	–5.82	–3.63	2.19

Measurements were carried out in CH_2Cl_2 of concentrations ~1×10^{-3} M, at a scan rate of 50 mVs^{-1} with Fc/Fc^+ employed as an internal standard, with data reported *vs.* SCE ($Fc/Fc^+ = 0.46$ V in CH_2Cl_2).[56] [a] Irreversible redox wave, onset value reported. [b] HOMO and LUMO energies were calculated following $E_{HOMO} = -[E^{ox\ vs.\ Fc/Fc+} + 5.1]$ eV, $E_{LUMO} = -[E^{red\ vs.\ Fc/Fc+} + 5.1]$ eV.[57]

In comparing the two bimetallic species a small increase in oxidative potential is again observed for the sulfone vs. sulfide complex (1.08 V for **Cu-Me-DPS** and 1.13 V for **Cu-Me-DPSO$_2$**), which is also attributed to electronic differences within the diimine ligand; the relatively attenuated influence in these cases is likely due to differences in the geometries of the two complexes where **Cu-Me-DPS** adopts a trigonal geometry and **Cu-Me-DPSO$_2$** a tetrahedral geometry. It has been shown that a stabilization of the tetrahedral geometry about the copper center is correlated to a more positive Cu^+/Cu^{2+} redox couple.[58] By adding substituents in the 6,6′-positions at the diimine ligand the flattening distortion is reduced upon oxidation. From the NMR studies it was deduced that in **Cu-Ph-DPS** the bulky phenyl substituents of the *N,N* ligand point inwards towards the copper center, thus helping to prevent rearrangement to the preferred square-planar coordination of Cu^{2+} upon oxidation of the copper centre. This stabilization of the tetrahedral Cu^{2+} state is seen in the oxidation potential of **Cu-Ph-DPS** (1.36 V), which is markedly higher than in the two unsubstituted tetrahedral complexes **Cu-DPS** and **Cu-DPSO$_2$**, and its sulfone derivative **Cu-Ph-DPSO$_2$** (1.18 V). **Cu-Ph-DPSO$_2$** has an almost identical oxidation potential to the other *N,O*-bound tetrahedral species **Cu-Me-DPSO$_2$**. All six complexes exhibit a reduction wave centered at –(0.85–1.01 V), which in previous studies has been assigned to a reduction centered on the bipyridyl

ligand.[55] The reductive wave is irreversible for all species, as is often the case for Cu(I) complexes.[55]

Solution-state Photophysical Properties

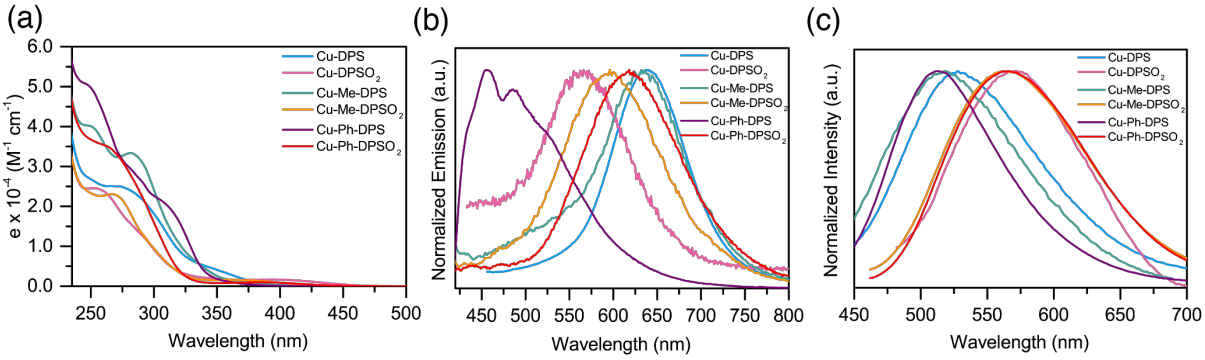

Figure 2. (a) Absorption and (b) emission spectra of Cu(I) complexes in CH_2Cl_2 solutions (concentrations: ~ 2 × 10^{-5} M, λ_{ex} = 370 nm); (b) Solid-state emission spectra of Cu(I) complexes as neat thin films drop-cast from MeOH on quartz substrates (λ_{ex} = 370 nm).

The absorption spectra of the pro-ligands **DPS**, **$DPSO_2$**, **Me-DPS**, **$Me\text{-}DPSO_2$**, **Ph-DPS** and **$Ph\text{-}DPSO_2$** in CH_2Cl_2 solutions are shown in Figure S65(a). The absorption spectra of **Me-DPS** and **$Me\text{-}DPSO_2$** are modestly red-shifted relative to those of their unsubstituted counterparts due to the electron-donating nature of the methyl substituents. Ligands **Ph-DPS** and **$Ph\text{-}DPSO_2$** are more significantly red-shifted due to the increased conjugation afforded by the phenyl rings in the 6- and 6'-positions. The absorption spectra of the six Cu(I) complexes in CH_2Cl_2 solutions are shown in Figure 2(a). All show intense high energy bands assigned to ligand-centered transitions and broad, lower energy bands in the range 325–450 nm due to metal-to-ligand charge transfer (MLCT) transitions to the diimine ligand, typical of $[Cu(P\text{^}P)(N\text{^}N)]^+$ complexes,[59] with the sulfone derivatives red-shifted compared to those of the sulfide analogs.

The photoluminescence spectra of the six complexes were collected in deaerated CH_2Cl_2 solutions (Figure 2(a)) and were found to be poorly emissive, presumably due to Jahn-Teller distortions in the excited-state leading to a quenching of the emission that is typical of many tetra-coordinated Cu(I) complexes.[16,39,60] Cu(I) complexes undergo a significant structural relaxation in the excited-state leaving a stabilized T_1 state. While the absorption occurs at the equilibrium geometry of the S_0 state, the emission occurs at the relaxed T_1 geometry and therefore determines to a large extent the energy of the radiative decay.[15,16,61]

Unsubstituted complex **Cu-DPS** is expected to show the largest geometrical change and therefore the greatest stabilization of the T_1 energy, evidenced by its lowest energy emission (λ_{PL} = 640 nm) of the six complexes. On oxidizing the ligand in **Cu-DPSO$_2$**, the emission undergoes a large hypsochromic shift to 566 nm. Of the methyl-substituted species, **Cu-Me-DPS** exhibits the lowest emission energy, similar to **Cu-DPS** (λ_{PL} = 632 nm) due to the distorted trigonal geometry about the copper center. The tetrahedral geometry of the excited-state of **Cu-Me-DPSO$_2$** can be stabilized through the introduction of the methyl groups in the 6,6′-positions of the bridging diimine ligand,[62] resulting in an emission at 596 nm. **Cu-Ph-DPS** shows a structured emission profile greatly blue-shifted relative to the emission of the other complexes (λ_{PL} = 456 nm), likely due to radiative decay from a ligand-centered (LC) transition. Its sulfone analogue, **Cu-Ph-DPSO$_2$** shows a red-shifted, featureless emission with a maximum at 618 nm. When compared with bimetallic **Cu-Me-DPSO$_2$** (its *N*,*O*-bound analogue), the emission of **Cu-Ph-DPSO$_2$** is only slightly bathochromically shifted despite the dramatically different coordination modes.

The stabilities of the dissolved complexes were probed in CH_2Cl_2 solutions. To test thermal stability the six Cu(I) species were dissolved in CH_2Cl_2 and stored in sealed vials under air and in the dark. Absorbance measurements were then obtained at t = 0, 2, 4, 6 and 24 h

(Figure S66). No decomposition was observed. In order to test photo-stability, **Cu-Ph-DPS** was irradiated with a UV hand lamp (λ_{ex} = 365 nm) for 0–10 min and the absorbance measured at different time points (Figure S67). No change was observed in the absorption spectra following irradiation, indicating the stability of the species to UV irradiation. Photoluminescence spectra of the six pro-ligands in CH_2Cl_2 were also collected (Figure S65) and all were found to emit at higher energies than their respective complexes. This demonstrates that the photoluminescence observed for the six complexes in CH_2Cl_2 is not due to free ligand fluorescence caused by instability.

Solid-State Photophysical Properties

The six Cu(I) species were each dissolved in MeOH, deposited onto quartz and left to air-dry, giving smooth drop-cast thin films from which photoluminescence data could be collected. At room temperature, all six Cu(I) species exhibit much more intense and blue-shifted emission when compared to measurements in CH_2Cl_2. This is characteristic of luminescent Cu(I) complexes and is attributed to the more rigid environment severely reducing the non-radiative decay channel resulting from the excited-state Jahn-Teller distortions. [3,62] The photoluminescence spectra of the six complexes as neat thin films are shown in Figure 2(b) and their photophysical properties summarized in Table 2. In both the monometallic (**Cu-DPS**, λ_{PL} = 525 nm; **Cu-DPSO$_2$**, λ_{PL} = 572 nm; **Cu-Ph-DPS**, λ_{PL} = 526 nm; **Cu-Ph-DPSO$_2$**, λ_{PL} = 562 nm) and bimetallic (**Cu-Me-DPS**, λ_{PL} = 518 nm; **Cu-Me-DPSO$_2$**, λ_{PL} = 557 nm) species, the emission of the sulfone analog is bathochromically shifted compared to the corresponding sulfide, regardless of coordination geometry. Functionalizing the diimine ligand with the electron-withdrawing sulfone reduces the electron density at the ortho-nitrogen atoms, which in turn results in a reduced σ-donating and increased π-accepting ligand about the copper

centre. This perturbation in the electronics of the ligand stabilizes the LUMO, reducing the HOMO–LUMO gap, and consequently results in red-shifted emission.

Table 2. Solid-state photophysical data of the six Cu(I) complexes, including ΔE_{ST} calculated from variable temperature steady-state and time-resolved photoluminescence spectra.

Complex	Steady-State λ_{PL} [nm] [a][b]		Steady-State ΔE_{ST} [eV] [a][b][c]	Time-Resolved ΔE_{ST} [eV] [d][e][f]	Calculated ΔE_{ST} [eV] [g]	Φ_{PL} [a][b]
	298 K	77 K				
Cu-DPS	525	536	0.04	0.03	0.13	0.04
Cu-DPSO$_2$	572	584	0.05	0.01	0.08	<0.01
Cu-Me-DPS	518	528	0.05	0.07	0.13	0.06
Cu-Me-DPSO$_2$	557	578	0.08	0.12	0.02	0.14
Cu-Ph-DPS	526	528	<0.01	0.06	0.21	0.07
Cu-Ph-DPSO$_2$	562	578	0.06	–	0.26	0.20

[a] Samples drop-cast onto quartz from MeOH. [b] λ_{exc} = 370 nm. [c] ΔE_{ST} calculated from difference between λ_{max} values. [d] Samples prepared as neat powders. [e] λ_{exc} = 340 nm. [f] ΔE_{ST} calculated from E_{0-0} values. E_{0-0} determined from emission onset at 298 K and 77 K. [g] Determined from TD-DFT calculations.

In order to gain further insight into the electronic properties of the species we turned to DFT calculations. Upon inspection of the frontier orbitals (Figure S70), for monometallic species **Cu-DPS**, **Cu-DPSO$_2$**, **Cu-Ph-DPS** and **Cu-Ph-DPSO$_2$** the HOMO is largely located on the 3d orbital of the copper(I) center and the coordinating DPEPhos ligand while the LUMO is mainly distributed over the N^N ligand, which is a distribution typical of Cu(I) monometallic complexes in the literature.[3] In the bimetallic complex **Cu-Me-DPS**, the HOMO is distributed over the 3d orbital of the copper(I) atom and the bridging DPEPhos ligand, with the LUMO located on the two distal dipyridyl ligands. In **Cu-Me-DPSO$_2$**, the HOMO is again located

across the copper(I) center and DPEPhos ligand, with the LUMO distributed mainly over the bridging **Me-DPSO$_2$** ligand. The HOMO–LUMO transitions are therefore assigned as metal-to-ligand charge transfer (MLCT). From TD-DFT calculations the resulting singlet states of the species are greater than 93% HOMO–LUMO character and so assigned as ^{1}MLCT states (Table S5). On analyzing the triplet states, the six species show greater than 88% HOMO–LUMO character and so are assigned as a mix of ^{3}MLCT/^{3}LLCT states. However, on analyzing the spin density plot of **Cu-Ph-DPS** (Figure S71) it can be seen that the transition is one of ^{3}LC character, and so the emitting state of this species is likely a combination of ^{3}MLCT/^{3}LLCT and ^{3}LC states.

In grouping the complexes into their relative geometries, trends in solid-state photoluminescence quantum yields (Φ_{PL}) can be seen. An increase in Φ_{PL} is seen in going from *N*,*N*-bound tetrahedral species **Cu-DPS** (0.04) and **Cu-DPSO$_2$** (<0.01), through the trigonal planar complexes **Cu-Me-DPS** (0.06) and **Cu-Ph-DPS** (0.07), to the most efficient emitters that are the *N*,*O*-bound tetrahedral complexes **Cu-Me-DPSO$_2$** (0.14) and **Cu-Ph-DPSO$_2$** (0.20). These values are modest and lower than for other DPEPhos-containing complexes that feature substituent groups in the 6,6′-positions of the diimine ligand (e.g., Φ_{PL} = 0.74 for [Cu(DPEPhos)(tmbpy)][BF$_4$] in the powder state).[34] It is possible that conformational flexibility about the sulfur center provides additional non-radiative decay pathways when compared to bpy-based N^N ligands. The extremely low Φ_{PL} of **Cu-DPSO$_2$** can be explained through the sulfone center causing additional electron-withdrawing character at the ligand, reducing the energy of the LUMO and thus the resulting emissive triplet state. From the oscillator strength data in Table S5, **Cu-DPSO$_2$** has the smallest value (f = 0.0012), which is a function of the very small exchange integral. This in turn correlates to a lower radiative rate (k_r) and thus a lower photoluminescence quantum yield is observed.

In the early 1960s, Hatchard and Parker observed TADF with a S_1–T_1 energy gap as high as ≈0.43 eV;[63] however, for TADF to be deemed efficient as is required in EL devices this energy gap should be around 0.1 eV.[3] This energy gap can be determined experimentally using variable-temperature steady-state photoluminescence spectroscopy. The emission from copper(I) systems at room temperature originates from a combination of both the S_1 and T_1 states. However, on cooling to 77 K the contribution from the T_1 state becomes much higher as the rISC rate is reduced. A red-shift in the emission profile is seen at low temperature and thus an estimation of singlet-triplet energy gap, ΔE_{ST}, can be made by taking the difference between the λ_{max} of emission at room temperature and at 77 K.[12] The PL spectra of the six copper(I) complexes were therefore collected at room temperature and 77 K (Figure 3) and ΔE_{ST} estimated from these results (Table 2). **Cu-DPS**, **Cu-DPSO$_2$**, **Cu-Me-DPS**, **Cu-Me-DPSO$_2$** and **Cu-Ph-DPSO$_2$** all exhibit a red-shift on cooling and ΔE_{ST} was found to be much less than 0.2 eV, which is sufficiently small to permit efficient rISC. Thus these complexes are candidates for emission via a TADF mechanism. Interestingly, the PL spectrum of **Cu-Ph-DPS** did not shift upon cooling, further indicating that the emission observed is likely a locally excited ligand-centred fluorescence.

Distinct spatial separation of the HOMO and LUMO is indicative of a small exchange integral and thus a small energy separation between ^{1}MLCT and ^{3}MLCT states.[3] From assessment of the calculated electron density distributions of the six species (Figure S70) it is apparent that the exchange integral will be small and so a relatively small ΔE_{ST} is predicted, indicative of TADF. Indeed, calculated ΔE_{ST} values obtained from the TD-DFT calculations are very small (0.02–0.26 eV, Table 2) and are consistent with the experimental data.

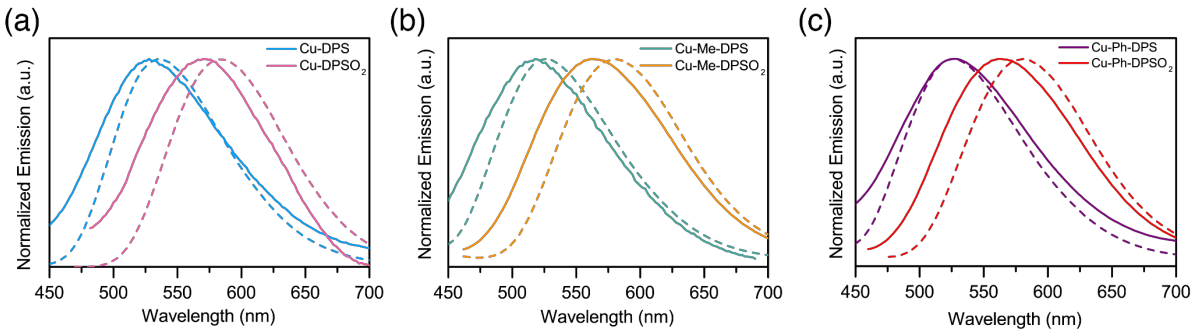

Figure 3. Solid-state emission spectra of (a) **Cu-DPS** and **Cu-DPSO$_2$**; (b) **Cu-Me-DPS** and **Cu-Me-DPSO$_2$**; (c) **Cu-Ph-DPS** and **Cu-Ph-DPSO$_2$** at room temperature (solid line) and 77 K (dashed line). Thin films drop-cast from MeOH onto quartz substrates (λ_{ex} = 370 nm).

In order to discern the radiative mechanism, variable temperature emission lifetimes were collected by time correlated single photon counting (TCSPC) over a temperature range of –196 to 28 °C (Figure 4, Figure S68 and Table S3). Generally, in emissive Cu(I) species, prompt fluorescence is not detected at low temperatures due to the non-negligible spin-orbit coupling constant of the copper. Instead a very bright, long-lived phosphorescence is seen. Upon increasing the temperature, the S_1 state can be populated, resulting in thermal activation of the rISC evidenced by a turn on of a blue-shifted delayed emission compared to the phosphorescence spectrum coupled with a drastic decrease in the emission lifetime. The decay time of a system with thermally equilibrated excited states is determined by a Boltzmann-type relationship, and thus variable temperature-dependent excited-state lifetime experiments of copper(I) species displaying TADF show a sigmoidal curve.[3]

The species studied here exhibit multi-exponential decay profiles, and when plotting the long lifetime components (which correspond to the thermalized emission of the triplet state), complexes **Cu-DPS**, **Cu-DPSO$_2$**, **Cu-Me-DPSO$_2$** and **Cu-Ph-DPSO$_2$** exhibit a sigmoidal profile, indicating the presence of TADF in their radiative mechanism. At low temperatures a plateau is observed, resulting from pure phosphorescence, with this plateau

most strongly seen in the sulfone species **Cu-Me-DPSO$_2$** and **Cu-Ph-DPSO$_2$**. **Cu-DPS** and **Cu-DPSO$_2$** exhibit a less pronounced plateau, and thus the nature of the emission at low temperatures in these complexes is likely an admixture of both TADF and phosphorescence. **Cu-Me-DPS** shows a temperature-dependent exponential decay of its longest emission component and the radiative pathway likely also contains a mixture of TADF and phosphorescence. It has been shown that –196 °C is not always sufficiently cold to isolate only the T_1 emission, and colder temperatures (e.g. 1.3 K) are often required to observe pure phosphorescence in Cu(I) complexes, and from this data ΔE_{ST} could then be determined using the Boltzmann-type equation.[3] Interestingly, **Cu-Ph-DPS** shows a decrease in the long lifetime component on cooling, indicating that this species is not a TADF emitter. At present, we are unsure as to the cause of this photophysical behavior.

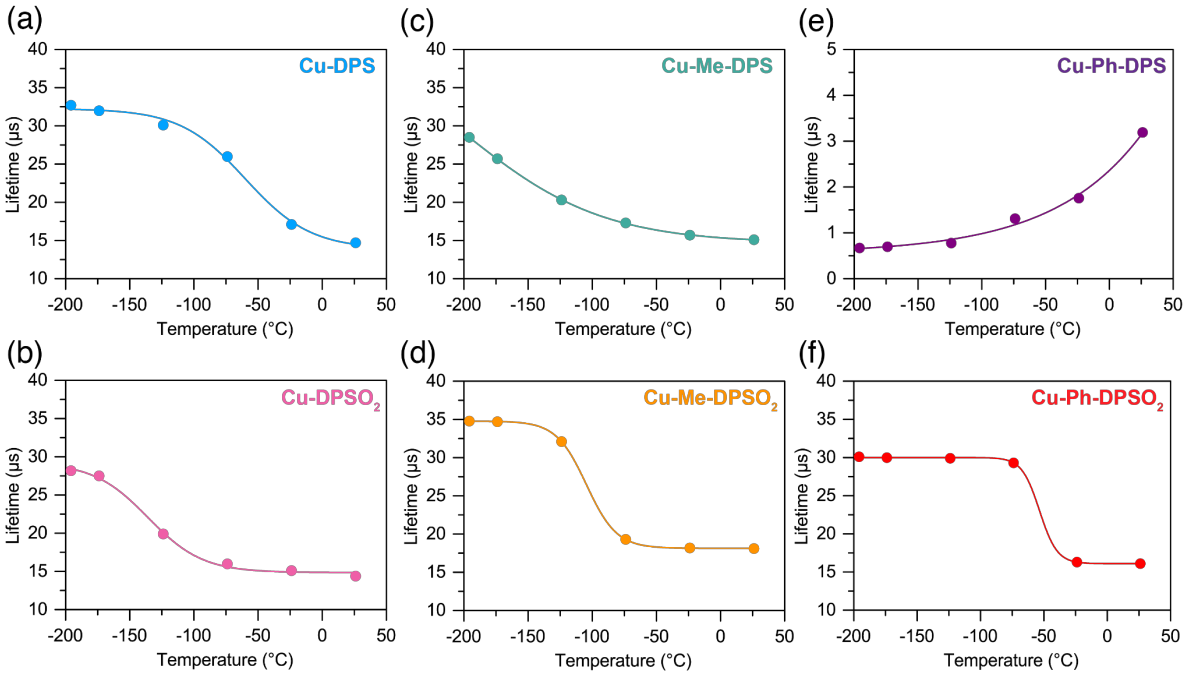

Figure 4. Solid-state photoluminescence lifetimes of (a) **Cu-DPS**; (b) **Cu-DPSO$_2$**; (c) **Cu-Me-DPS**; (d) **Cu-Me-DPSO$_2$**; (e) **Cu-Ph-DPS**; and (f) **Cu-Ph-DPSO$_2$** from –196 to 25 °C. Samples drop-cast as neat thin films from MeOH on quartz slides (λ_{ex} = 370 nm).

Time-resolved Photophysical Properties

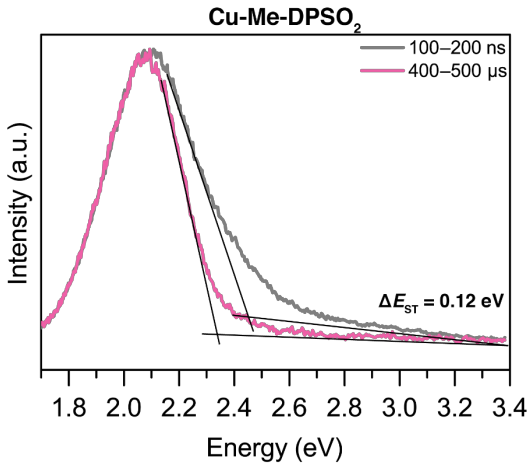

Figure 5. Time-resolved solid-state photoluminescence spectrum of **Cu-Me-DPSO$_2$** at 77 K. The grey trace represents emission from the S_1 state, and the pink trace emission from the T_1 state. Black lines indicate the determination of the zero-zero energy (E_{0-0}). Sample prepared as a neat powder (λ_{ex} = 340 nm).

In order to more accurately determine the ΔE_{ST} values, time-resolved photoluminescence spectroscopy was employed (Table 2, Figure 5, Figure S69).[64] Samples were prepared as neat powders and cooled to 77 K, following which photoluminescence spectra for transitions emanating from the S_1 state (100–200 ns time regime, grey traces) and the T_1 state (400–500 µs time regime, pink traces) could be obtained. In all instances a shift to lower energy is seen when monitoring the longer time component, indicative of emission from a lower-energy state. By determining the zero-zero energy (E_{0-0}) from the onset of each excited-state transition (represented by the black lines in Figure S69), ΔE_{ST} was calculated for each complex. **Cu-DPS** (0.03 eV), **Cu-DPSO$_2$** (0.01 eV), **Cu-Me-DPS** (0.07 eV), **Cu-Me-DPSO$_2$**

(0.12 eV, Figure 5) and **Cu-Ph-DPS** (0.06 eV) all have S_1–T_1 energy gaps that are sufficiently small in the powder and thus are likely to emit in part from a TADF mechanism. Unfortunately, the presence of small amounts of $[Cu(DPEPhos)_2][BF_4]$ impurity was observed in the prompt time-resolved spectrum of **Cu-Ph-DPSO$_2$** and so a E_{0-0} value could not be determined in this case. Efforts to re-synthesize the complex did not result in the removal of this impurity. $[Cu(DPEPhos)_2][BF_4]$ is not seen in the NMR data, and is therefore determined to be in very low concentrations. Additionally, its appearance in the time-resolved data is only seen in the prompt time regime and is not present in the steady-state emission data (Figure 3(c)) and so we are confident that the minor impurity does not affect the emission lifetime discussion above. Comparisons of the time-resolved data with the steady-state data are presented in Table 2, illustrating the ΔE_{ST} values are close between the two techniques.

CONCLUSIONS

Six heteroleptic Cu(I) complexes of the class $[Cu(DPEPhos)(N^N)][BF_4]$ (where N^N = sulfur-bridged dipyridyl ligands) are reported and are functionalized either with or without methyl or phenyl substituents in the 6,6′-positions of the pyridyl rings, and sulfide or sulfone oxidation states at the sulfur center. Single crystal structures of **Cu-DPS**, **Cu-DPSO$_2$** are bound in a *N*,*N* mode at the diimine ligand and are coordinated in a distorted tetrahedral geometry. However, upon introducing additional bulk with methyl groups the steric constraints about the copper center become too great and dimeric structures result. **Cu-Me-DPS** is a bimetallic species that adopts a trigonal geometry with a bridging DPEPhos ligand, whereas **Cu-Me-DPSO$_2$** forms a bimetallic species with the diimine moiety acting as a bridging ligand linking the two copper atoms. Interestingly, when the steric constraints are increased further by substitution of phenyl rings in the 6,6′-positions of the pyridyl rings, monometallic species are

again isolated. **Cu-Ph-DPS** adopts a distorted trigonal geometry with the diimine ligand bound through only one pyridyl nitrogen; however, on increasing the oxidation state of the sulfur bridge to sulfone in **Cu-Ph-DPSO$_2$**, an accessible binding site is created, causing the **Ph-DPSO$_2$** ligand to bind in a *N*,*O* fashion forming a tetrahedral geometry about the copper atom.

The complexes are all weakly emissive in solution, but are more strongly emissive in the solid state, with photoluminescence quantum yields of up to 0.20 for the most sterically encumbered complex, **Cu-Ph-DPSO$_2$**. The sulfone complexes (**Cu-DPSO$_2$**, **Cu-Me-DPSO$_2$** and **Cu-Ph-DPSO$_2$**) show red-shifted emission profiles when compared to their sulfide counterparts (**Cu-DPS**, **Cu-Me-DPS** and **Cu-Ph-DPS**) due to the electron withdrawing nature of the sulfone and its impact on the donating strength of the pyridine rings of the diimine ligand. Steady-state and time-resolved photoluminescence spectroscopies were employed to determine ΔE_{ST}. In all six complexes a $\Delta E_{ST} < 0.08$ eV indicating that efficient reverse intersystem crossing (rISC) would occur. Variable temperature time-correlated single photon counting (TCSPC) was used to further probe the radiative mechanism, with complexes **Cu-DPS**, **Cu-DPSO$_2$**, **Cu-Me-DPS**, **Cu-Me-DPSO$_2$** and **Cu-Ph-DPSO$_2$** decaying via a largely TADF mechanism. **Cu-Ph-DPS** showed photoluminescence properties consistent with that of a triplet ligand-centered (^{3}LC) emission.

Here, we have shown that with changes in steric constraints and sulfur oxidation state a variety of different complex geometries can be obtained. **Cu-Me-DPS** represents the first examples of a dimetallic Cu(I) species bridged by a DPEPhos ligand, and **Cu-Me-DPSO$_2$** and **Cu-Ph-DPSO$_2$** represent the first examples of sulfone-based *N*,*O*-bound diimine ligands. **Cu-Ph-DPSO$_2$** could show promise for application in LEECs, and the novel binding modes seen in the complex could open avenues towards interesting, luminescent coordination polymers.

EXPERIMENTAL SECTION

General. All experiments were conducted in atmospheric conditions unless otherwise stated. Solvents used for synthesis were reagent grade and were used without any further purification. HPLC grade solvents were used for spectroscopic studies. 2-bromo-6-methylpyridine and niobium carbide (NbC) were purchased from Alfa Aesar, $[Cu(MeCN)_4][BF_4]$ and 30% H_2O_2 solutions were purchased from Sigma-Aldrich, and thiourea from TCI. All reagents were used as received. Bis(pyridin-2-yl)sulfane (**DPS**) and 2,2′-sulfonyldipyridine (**$DPSO_2$**) were synthesized using the methods previously reported by our group,[44] and 2-bromo-6-phenylpyridine was prepared according to the literature.[65]

Spectroscopy. ^1H, $^{13}C\{^1H\}$, $^{31}P\{^1H\}$, COSY, NOESY, HSQC and HMBC NMR spectra were collected using a Bruker AV-400 or AV-600 spectrometer and referenced first to TMS and then to the residual protonated solvent peak. NMR solvents (Aldrich or Cambridge Isotope Laboratories) were used as received. Electrospray ionization mass spectrometry data was obtained using a Bruker Esquire LC ion trap mass spectrometer and elemental analysis determined using a Thermo Flash 2000 Elemental Analyzer. Infrared spectroscopy was performed on an attenuated total reflection (ATR) crystal using a Perkin-Elmer Frontier FT-IR spectrometer. UV-vis absorption spectra were recorded on a Varian-Cary 5000 UV-Vis-near-IR spectrophotometer. Fluorescence data were collected on a Photon Technology International (PTI) QuantaMaster 50 fluorimeter fitted with an integrating sphere, double excitation monochrometer and utilizing a 75 W Xe arc lamp as the source. Emission lifetime data were collected using a Horiba Yvon Fluorocube TCSPC apparatus fitted with an inline Stanford Research Systems DG535 digital delay generator. A 370 nm NanoLED was used as the excitation source, pulsing at a repetition rate of 10 kHz and with a lifetime of 1.2 ns. Broadband emission was monitored by a Horiba Jobin Yvon TBX Picosecond Photon Detection module at the desired wavelengths using a 450 nm low-pass filter. The lifetime data were fitted using

the DAS6 Data Analysis software package. Low temperature studies were conducted with an Oxford Instruments Optistat DN using an ITC610 temperature controller. Solution spectra were collected using 1 cm^2 quartz cells (Starna Cells) and solid thin films were prepared by depositing from MeOH onto quartz slides (Ted Pella, Inc.) with the solvent left to evaporate in ambient conditions, leaving a dry film with a smooth surface. Time-resolved phosphorescence and prompt fluorescence spectra were excited by a Light Conversion Orpheus-N (model PN13F1) optical parametric amplifier generating ~150 fs pulses at 340 nm. The emission was focused onto a Chromex 250is spectrograph and detected with a gated iCCD camera (Stanford Computer Optics, 4Picos) having sub-nanosecond resolution. Long time spectra were integrated by iCDD between 400 μs–500 μs after the laser excitation, and short time spectra integrated by iCDD between 100 ns–200 ns after excitation.

Electrochemical Methods. Cyclic voltammetry (CV) measurements were performed at room temperature with an electrochemical analyzer potentiostat model 620E from CH Instruments at a sweep rate of 50 mV/s. Differential pulse voltammetry (DPV) was conducted with an increment potential of 0.004 V and a pulse amplitude, width, and period of 50 mV, 0.05, and 0.5 s, respectively. Solutions for CV and DPV were prepared in CH_2Cl_2 of concentrations ~1 × 10^{-3} M and degassed with CH_2Cl_2-saturated N_2 bubbling for 10 min prior to scanning. Tetra(*n*-butyl)ammonium hexafluorophosphate ($TBAPF_6$; ca. 0.1 M in CH_2Cl_2) was used as the supporting electrolyte. A silver wire was used as the pseudoreference electrode; a glassy-carbon electrode was used for the working electrode and a Pt wire was used as the counter electrode. The redox potentials are reported relative to a standard calomel electrode (SCE) electrode with a ferrocene/ferrocenium (Fc/Fc^+) redox couple as an internal reference (0.46 V vs SCE for CH_2Cl_2).

X-Ray Crystallography. SCXRD raw data were collected on a Bruker APEX DUO diffractometer using graphite monochromated MoKα radiation (λ = 0.71073) at 90 K and to a resolution of 0.77 Å. The data elaboration was performed with the software APEX2.[66] Structures were solved using SUPERFLIP[67] and refined using full-matrix least-squares on F^2 within the CRYSTALS[68] suite. Hydrogen atoms were initially refined with restraints on bond lengths and angles, after which the positions were used as the basis for a riding model.[69] All non-hydrogen atoms were refined anisotropically.

Computational Details. Density functional theory (DFT) calculations were carried out using the Gaussian 16 Rev.A03 suite of programs. The B3LYP functional[70-72] with 6-31G** basis set (for C, H, S N P and O atoms) and the LANL2DZ effective-core pseudopotential (for Cu)[73] was employed to optimize the geometry of the ground-states (S_0) of all complexes with input structures extracted from the X-ray crystallographic data, and the geometry of the lowest triplet states (T_1) were calculated by unrestricted methods. Time-dependent DFT (TD-DFT) calculations were also performed using the same method to understand the vertical transition of the ground state (S_0) and the nature of first singlet (S_1) and triplet excited states (T_1).[74-76] Dispersion corrections were employed for all geometry optimizations using the D3 correction method of Grimme *et al.*[77]

Synthesis

Bis(6-methylpyridin-2-yl)sulfane (**Me-DPS**). 2-Bromo-6-methylpyridine (0.66 mL, 5.81 mmol, 1.0 equiv.) was added to a solution of thiourea (0.21 g, 2.76 mmol, 0.48 equiv.) in 100 mL of EtOH under an N_2 atmosphere and heated to reflux for 36 h. The reaction mixture was cooled to room temperature, the solvent removed under reduced pressure and the resultant residue dissolved in CH_2Cl_2 (20 mL) and washed with water (3 × 20 mL) and brine (1 × 50

mL). The organic layer was dried with $MgSO_4$, filtered and the CH_2Cl_2 removed *in vacuo*. The crude product was purified over silica gel using a solvent gradient from 1:0 CH_2Cl_2:MeOH to 9:1 CH_2Cl_2:MeOH, yielding a brown oil (0.558 g, 2.72 mmol, 99%). ^{1}H NMR (400 MHz, CD_2Cl_2) δ 7.50 (t, *J* = 7.7 Hz, 2H), 7.19 (dt, *J* = 7.9, 0.8 Hz, 2H), 7.02 (ddd, *J* = 7.6, 0.9, 0.5 Hz, 2H), 2.50 (s, 6H). ^{13}C{^{1}H} NMR (CD_2Cl_2, 100 MHz) δ 159.82, 156.80, 137.69, 123.05, 121.67, 24.62. ESI-HR MS: Calcd. for $C_{12}H_{13}N_2S$: 217.0799; Found: 217.0798 $[M+H]^+$

6,6'-Sulfonylbis(2-methylpyridine (**Me-DPSO$_2$**). A round-bottomed flask was charged with **Me-DPS** (0.167 g, 0.772 mmol, 1.0 equiv.) and NbC (0.020 g, 0.193 mmol, 0.25 equiv.). 10 mL EtOH and 30% aqueous solution of H_2O_2 (1.09 mL, 11.6 mmol, 15.0 equiv.) were added and the reaction mixture was heated to 60 ºC for 12 h. The mixture was cooled to room temperature, diluted with saturated $Na_2S_2O_3$ (10 mL) and extracted with CH_2Cl_2 (3 × 10 mL). The combined organics were dried over $MgSO_4$, filtered and the solvent removed *in vacuo* yielding a white powder that required no further purification (0.190 g, 0.765 mmol, 99%). ^{1}H NMR (400 MHz, CD_2Cl_2) δ 8.07 (d, *J* = 7.7 Hz, 2H), 7.85 (t, *J* = 7.8 Hz, 2H), 7.36 (d, *J* = 7.8 Hz, 2H), 2.51 (s, 6H). ^{13}C{^{1}H} NMR (101 MHz, CD_2Cl_2) δ 160.67, 156.90, 138.43, 127.71, 121.54, 24.53. ESI-HR MS: Calcd. for $C_{12}H_{12}N_2O_2SNa$: 271.0517; Found: 271.0520 $[M+Na]^+$.

Bis(6-phenylpyridin-2-yl)sulfane (**Ph-DPS**). 2-Bromo-6-phenylpyridine (0.916 g, 2.95 mmol, 2.0 equiv.) and thiourea (0.150 g, 1.97 mmol, 1.0 equiv.) were dissolved in EtOH (50 mL) under and N_2 atmosphere and heated to reflux for 72 h. The reaction mixture was then cooled to room temperature, the solvent removed *in vacuo* and the resultant crude product dissolved CH_2Cl_2 (20 mL) and washed with water (3 × 20 mL) and brine (1 × 50 mL). The organic layer was dried with $MgSO_4$, filtered and the CH_2Cl_2 removed under reduced pressure, following which the crude material was purified over a silica gel column using CH_2Cl_2. The

pure product was isolated as an off-white powder (0.238 g, 0.699 mmol, 36%). ^{1}H NMR (400 MHz, CD_2Cl_2) δ 8.03 – 7.97 (m, 4H), 7.72 (t, *J* = 7.7 Hz, 2H), 7.66 (dd, *J* = 7.8, 1.0 Hz, 2H), 7.50 – 7.39 (m, 8H). ^{13}C{^{1}H} NMR (101 MHz, CD_2Cl_2) δ 158.02, 157.30, 139.05, 138.22, 129.79, 129.23, 127.34, 124.65, 118.70. ESI-HR MS: Calcd. for $C_{22}H_{17}N_2S$: 341.1112; Found: 341.1118 $[M+H]^+$.

6,6'-Sulfonylbis(2-phenylpyridine) (Ph-DPSO$_2$). To a round-bottomed flask was added **Ph-DPS** (0.102 g, 0.300 mmol, 1.0 equiv.), NbC catalyst (0.008 g, 0.075 mmol, 0.25 equiv.) and EtOH (15 mL). A 30% aqueous solution of H_2O_2 (0.45 mL, 4.50 mmol, 15.0 equiv.) was added and the reaction mixture heated to 60 ºC for 12 h. The solution was cooled to room temperature, diluted with saturated $Na_2S_2O_3$ (15 mL) and extracted with CH_2Cl_2 (3 × 10 mL). The combined organics were washed with brine (30 mL), dried over $MgSO_4$, filtered and the CH_2Cl_2 removed *in vacuo* yielding a white powder that required no further purification (0.111 g, 0.300 mmol, 100%). ^{1}H NMR (400 MHz, CD_2Cl_2) δ 8.28 (dd, *J* = 7.7, 0.9 Hz, 2H), 8.07 (t, *J* = 7.9 Hz, 2H), 7.95 (dd, *J* = 8.1, 0.9 Hz, 2H), 7.94 – 7.88 (m, 4H), 7.47 – 7.39 (m, 6H). ^{13}C{^{1}H} NMR (101 MHz, CD_2Cl_2) δ 158.51, 157.64, 139.34, 137.76, 130.52, 129.38, 127.52, 124.27, 122.50. ESI-HR MS: Calcd. for $C_{22}H_{17}N_2O_2S$: 373.1011; Found: 373.1002 $[M+H]^+$.

[Cu(DPEPhos)(DPS)][BF$_4$] (Cu-DPS). $[Cu(MeCN)_4]BF_4$ (0.092 g, 0.292 mmol, 1.0 equiv.) and DPEPhos (0.158 g, 0.292 mmol, 1.0 equiv.) were dissolved in 12 mL CH_2Cl_2 and stirred at room temperature for 2 h, after which **DPS** (0.055 g, 0.292 mmol, 1.0 equiv.) was added and the solution left to stir for a further 1 h. The reaction mixture was then concentrated *in vacuo*, the product precipitated with Et_2O, filtered and washed with Et_2O, yielding an off-white powder that required no further purification (0.214 g, 0.244 mmol, 84%). ^{1}H NMR (400 MHz, CD_3OD) δ 8.16 – 8.10 (m, 2H), 7.90 – 7.81 (m, 4H), 7.39 – 7.19 (m, 22H), 7.14 – 7.08 (m,

2H), 7.05 (td, J = 7.6, 1.1 Hz, 2H), 6.99 (dtd, J = 8.2, 2.5, 1.0 Hz, 2H), 6.82 (dtd, J = 7.8, 4.0, 1.6 Hz, 2H). $^{13}C\{^{1}H\}$ NMR (101 MHz, CD_3OD) δ 159.11, 154.90, 152.31, 140.64, 135.02, 134.74 (t, J = 8.1 Hz), 133.41, 132.22 (t, J = 16.5 Hz), 131.47, 130.29, 129.98, 126.30, 125.92 (t, J = 14.4 Hz), 125.41, 121.69. $^{31}P\{^{1}H\}$ NMR (162 MHz, CD_3OD) δ –14.20. ESI-HR MS Calcd. for $C_{46}H_{36}N_2OP_2S^{63}Cu$: 789.1320; Found: 789.1323 $[M–BF_4]^+$. Elemental Analysis: Calcd. $C_{46}H_{36}BF_4N_2OP_2SCu$: C, 62.99; H, 4.14; N, 3.19; S, 3.65. Found: C, 62.71; H, 4.26; N, 3.15; S, 3.64.

[Cu(DPEPhos)(DPSO$_2$)][BF$_4$] (**Cu-DPSO$_2$**). A solution of $[Cu(MeCN)_4]BF_4$ (0.079 g, 0.250 mmol, 1.0 equiv.) and DPEPhos (0.134 g, 0.250 mmol, 1.0 equiv.) in 12 mL CH_2Cl_2 was stirred at room temperature for 2 h, after which **DPSO$_2$** (0.055 g, 0.250 mmol, 1.0 equiv.) was added and the solution left to stir for a further 1 h. The reaction mixture was then concentrated under reduced pressure, the product precipitated with Et_2O, filtered and washed with Et_2O, giving a yellow powder (0.210 g, 0.231 mmol, 92%). ^{1}H NMR (400 MHz, CD_3OD) δ 8.52 (d, J = 4.8 Hz, 2H), 8.36 (d, J = 7.9 Hz, 2H), 8.14 (td, J = 7.8, 1.6 Hz, 2H), 7.54 (ddd, J = 7.7, 4.9, 1.2 Hz, 2H), 7.46 – 7.37 (m, 4H), 7.31 (ddt, J = 10.2, 7.3, 2.7 Hz, 18H), 7.02 (td, J = 7.6, 1.1 Hz, 2H), 6.97 (dtd, J = 8.2, 2.5, 1.0 Hz, 2H), 6.75 (dtd, J = 7.9, 4.1, 1.6 Hz, 2H). $^{13}C\{^{1}H\}$ NMR (101 MHz, CD_3OD) δ 159.13 (t, J = 5.9 Hz), 157.31, 152.08, 140.67, 135.28, 134.81 (t, J = 8.3 Hz), 133.31, 132.00 (t, J = 17.2 Hz), 131.53, 130.02 (t, J = 4.9 Hz), 129.64, 126.13, 125.54, 125.31 (t), 121.44. $^{31}P\{^{1}H\}$ NMR (162 MHz, CD_3OD) δ –17.56. ESI-HR MS Calcd. for $C_{46}H_{36}N_2O_3P_2S^{63}Cu$: 821.1225; Found: 821.1218 $[M–BF_4]^+$. Elemental Analysis: Calcd. $C_{46}H_{36}BF_4N_2O_3P_2SCu$: C, 60.77; H, 3.99; N, 3.08; S, 3.53. Found: C, 60.44; H, 4.24; N, 2.76; S, 3.41.

[(Me-DPS)Cu(DPEPhos)Cu(Me-DPS)][BF_4]$_2$ (Cu-Me-DPS). [$Cu(MeCN)_4$]BF_4 (0.176 g, 0.559 mmol, 2.0 equiv.) and DPEPhos (0.140 g, 0.278 mmol, 1.0 equiv.) were dissolved in 15 mL CH_2Cl_2 and stirred at room temperature for 2 h, after which **Me-DPS** (0.121 g, 0.559 mmol, 2.0 equiv.) was added and the solution left to stir for a further 1 h. The reaction mixture was then concentrated *in vacuo*, the product precipitated with Et_2O, filtered and washed with Et_2O, yielding an off-white powder that required no further purification (0.290 g, 0.228 mmol, 82%). ^{1}H NMR (400 MHz, CD_3OD) δ 7.91 (br s, 8H), 7.51 (br m, 2H) 7.39 (m, 8H), 7.28 (t, *J* = 7.5 Hz, 8H), 7.14 (m, 10H), 7.02 (t, *J* = 7.5 Hz, 2H), 6.64 (dtd, *J* = 5.9, 4.1, 1.5 Hz, 2H), 2.21 (br s, 12H). ^{13}C{^{1}H} NMR (101 MHz, CD_3OD) δ 159.33, 135.54, 134.44 (t), 133.63, 131.74, 131.30 (t, *J* = 19.6 Hz), 130.14 (t, *J* = 5.0 Hz), 126.31, 124.36, 121.40. ^{31}P{^{1}H} NMR (162 MHz, CD_3OD) δ –15.83. Elemental Analysis: Calcd. $C_{60}H_{52}B_2F_8N_4OP_2S_2Cu_2$: C, 56.66; H, 4.12; N, 4.41; S, 5.04. Found: C, 56.64; H, 4.12; N, 4.40; S, 5.10.

[(DPEPhos)Cu(Me-DPSO$_2$)Cu(DPEPhos)][BF_4]$_2$ (Cu-Me-DPSO$_2$). [$Cu(MeCN)_4$]BF_4 (0.064 g, 0.202 mmol, 2.0 equiv.) and DPEPhos (0.109 g, 0.202 mmol, 1.0 equiv.) were dissolved in 10 mL CH_2Cl_2 and stirred at room temperature for 2 h, after which **Me-DPSO$_2$** (0.025 g, 0.101 mmol, 1.0 equiv.) was added and the solution left to stir for a further 1 h. The reaction mixture was then concentrated *in vacuo*, the product precipitated with Et_2O, filtered and washed with Et_2O, yielding a yellow powder that required no further purification (0.157 g, 0.097 mmol, 96%). ^{1}H NMR (400 MHz, CD_3OD) δ 8.00 (d, *J* = 7.5 Hz, 4H), 7.53 (d, *J* = 7.2 Hz, 2H), 7.47 – 7.40 (m, 8H), 7.39 – 7.27 (m, 36H), 7.00 (t, *J* = 7.4 Hz, 8H), 6.69 (dtd, *J* = 8.0, 4.0, 1.6 Hz, 4H), 2.26 (s, 6H). ^{13}C{^{1}H} NMR (101 MHz, CD_3OD) δ ^{13}C{^{1}H} NMR (101 MHz, CD_3OD) δ 161.65, 159.34 (t), 140.50, 135.41, 134.77 (t, *J* = 8.3 Hz), 133.25, 132.20 (t, *J* = 17.6 Hz), 131.58, 130.02 (t, *J* = 4.9 Hz), 126.02, 124.96 (t, *J* = 15.5 Hz), 122.78, 121.45, 24.28. ^{31}P{^{1}H} NMR (162 MHz, CD_3OD) δ –18.44. Elemental Analysis: Calcd.

$C_{84}H_{68}B_2F_8N_2O_4P_4SCu$: C, 62.04; H, 4.22; N, 1.72; S, 1.97. Found: C, 62.02; H, 4.55; N, 1.60; S, 1.93.

[Cu(DPEPhos)(Ph-DPS)][BF_4] (**Cu-Ph-DPS**). To a round-bottomed flask was added [$Cu(MeCN)_4$]BF_4 (0.046 g, 0.147 mmol, 1.0 equiv.) and DPEPhos (0.079 g, 0.147 mmol, 1.0 equiv.). The solids were dissolved in CH_2Cl_2 (10 mL) and stirred at room temperature for 2 h, after which **Ph-DPS** (0.050 g, 0.147 mmol, 1.0 equiv.) was added and the solution left to stir for a further 1 h. The reaction mixture was then concentrated under reduced pressure, and the product precipitated out through the addition of Et_2O. The precipitate was filtered and washed with Et_2O, yielding an off-white powder that required no further purification (0.108 g, 0.105 mmol, 71%). ^{1}H NMR (400 MHz, CD_3OD) δ 7.83 (t, *J* = 7.8 Hz, 2H), 7.74 (ddd, *J* = 8.6, 5.5, 1.3 Hz, 6H), 7.45 – 7.25 (m, 14H), 7.22 (t, *J* = 7.5 Hz, 8H), 7.14 – 7.06 (m, 2H), 7.03 (q, *J* = 6.2 Hz, 8H), 6.96 (td, *J* = 7.6, 1.1 Hz, 2H), 6.55 (dtd, *J* = 8.0, 4.3, 1.6 Hz, 2H). ^{13}C{^{1}H} NMR (101 MHz, CD_3OD) δ 158.46, 157.95, 154.81, 138.95, 138.27, 134.20, 133.17 (t, *J* = 7.9 Hz), 132.20, 130.32, 130.02, 129.68, 128.89, 128.80 (t, *J* = 4.9 Hz), 126.60, 125.56, 125.43, 124.81, 120.47, 120.10. ^{31}P{^{1}H} NMR (162 MHz, CD_3OD) δ –16.23. ESI-HR MS Calcd. for $C_{58}H_{44}N_2OP_2S^{63}Cu$: 941.1946; Found: 941.1939 $[M–BF_4]^+$. Elemental Analysis: Calcd. $C_{58}H_{44}BF_4N_2OP_2SCu$: C, 67.68; H, 4.31; N, 2.72; S, 3.11. Found: C, 66.38; H, 4.09; N, 2.55; S, 2.97.

[Cu(DPEPhos)(Ph-DPSO_2)][BF_4] (**Cu-Ph-DPSO_2**). [$Cu(MeCN)_4$]BF_4 (0.025 g, 0.081 mmol, 1.0 equiv.) and DPEPhos (0.044 g, 0.081 mmol, 1.0 equiv.) were dissolved in 12 mL CH_2Cl_2 and stirred at room temperature for 2 h, after which **Ph-DPSO_2** (0.030 g, 0.081 mmol, 1.0 equiv.) was added and the solution left to stir for a further 1 h. The reaction mixture was then concentrated *in vacuo*, the product precipitated with Et_2O, filtered and washed with Et_2O,

yielding an off-white powder that required no further purification (0.052 g, 0.049 mmol, 61%). ^{1}H NMR (600 MHz, CD_2Cl_2) δ 8.02 (t, *J* = 7.9 Hz, 1H), 7.90 (dd, *J* = 8.0, 1.0 Hz, 1H), 7.87 (d, *J* = 7.9 Hz, 1H), 7.57 – 7.50 (m, 2H), 7.35 (d, *J* = 7.6 Hz, 4H), 7.28 (q, *J* = 7.4 Hz, 3H), 7.22 (t, *J* = 7.6 Hz, 8H), 7.07 (dd, *J* = 19.4, 11.6 Hz, 10H), 6.97 (t, *J* = 7.5 Hz, 2H), 6.94 (d, *J* = 8.0 Hz, 2H), 6.67 (q, *J* = 6.2, 5.1 Hz, 2H). ^{13}C{^{1}H} NMR (151 MHz, CD_2Cl_2) δ 160.12, 158.13, 155.00, 140.65, 137.42, 134.83, 133.91, 132.61, 131.20, 130.99, 130.29, 129.62, 129.47 (t, *J* = 4.9 Hz), 127.96, 127.50, 125.44, 123.58, 123.04, 120.45. ^{31}P{^{1}H} NMR (162 MHz, CD_2Cl_2) δ –15.42. ESI-HR MS Calcd. for $C_{58}H_{44}N_2O_3P_2S^{63}Cu$: 973.1844; Found: 973.1852 $[M–BF_4]^+$.

ASSOCIATED CONTENT

Supporting Information

The supporting information is available free of charge on the ACS Publications website at DOI:

Characterization data (NMR, mass spectrometry and elemental analysis), crystallographic data, electrochemical data, photophysical data (absorption, TCSPC and time-resolved emission spectra) and theoretical calculations.

AUTHOR INFORMATION

Corresponding Author

*E-mail for M.O.W.: mwolf@chem.ubc.ca

Notes

The authors declare no competing financial interest.

ACKNOWLEDGEMENTS

C.M.B. thanks Dr. Maria B. Ezhova for helpful discussions regarding NMR spectra, and Dr. Saeid Kamal for assistance with the TCSPC data. C.M.B. and M.O.W. acknowledge the

Natural Sciences and Engineering Research Council of Canada (NSERC) and the Peter Wall Institute for Advanced Studies for financial support and the Laboratory for Advanced Spectroscopy for Imaging Research (LASIR) for facilities access. Z.X. thanks Compute Canada for computing resources for DFT calculations. C.L. thanks the Prof. & Mrs. Purdie Bequests Scholarship and AstraZeneca PhD Studentship. E.Z.-C. and I.D.W.S thank EPSRC (grants EP/R035164/1 and EP/L017008/1) for financial support.

REFERENCES

(1) Hagfeldt, A.; Boschloo, G.; Sun, L.; Kloo, L.; Pettersson, H. Dye-Sensitized Solar Cells. *Chem. Rev.* **2010**, *110*, 6595–6663.

(2) Prier, C. K.; Rankic, D. A.; MacMillan, D. W. C. Visible Light Photoredox Catalysis with Transition Metal Complexes: Applications in Organic Synthesis. *Chem. Rev.* **2013**, *113*, 5322–5363.

(3) Czerwieniec, R.; Leitl, M. J.; Homeier, H. H. H.; Yersin, H. Cu(I) Complexes – Thermally Activated Delayed Fluorescence. Photophysical Approach and Material Design. *Coord. Chem. Rev.* **2016**, *325*, 2–28.

(4) Farinola, G. M.; Ragni, R. Electroluminescent Materials for White Organic Light Emitting Diodes. *Chem. Soc. Rev.* **2011**, *40*, 3467–3482.

(5) Chi, Y.; Chou, P.-T. Transition-Metal Phosphors with Cyclometalating Ligands: Fundamentals and Applications. *Chem. Soc. Rev.* **2010**, *39*, 638–655.

(6) Henwood, A. F.; Zysman-Colman, E. Luminescent Iridium Complexes Used in Light-Emitting Electrochemical Cells (LEECs). *Top. Curr. Chem.* **2016**, *374*, 36.

(7) Housecroft, C. E.; Constable, E. C. Over the LEC Rainbow: Colour and Stability Tuning of Cyclometallated Iridium(III) Complexes in Light-Emitting Electrochemical Cells. *Coord. Chem. Rev.* **2017**, *350*, 155–177.

(8) Costa, R. D.; Ortí, E.; Bolink, H. J.; Graber, S.; Schaffner, S.; Neuburger, M.; Housecroft, C. E.; Constable, E. C. Archetype Cationic Iridium Complexes and Their Use in Solid-State Light-Emitting Electrochemical Cells. *Adv. Funct. Mater.* **2009**, *19*, 3456–3463.

(9) Xu, H.; Chen, R.; Sun, Q.; Lai, W.; Su, Q.; Huang, W.; Liu, X. Recent Progress in Metal-Organic Complexes for Optoelectronic Applications. *Chem. Soc. Rev.* **2014**, *43*, 3259–3302.

(10) Cebrián, C.; Mauro, M. Recent Advances in Phosphorescent Platinum Complexes for Organic Light-Emitting Diodes. *Beilstein J. Org. Chem.* **2018**, *14*, 1459–1481.

(11) Bizzarri, C.; Spuling, E.; Knoll, D. M.; Volz, D.; Bräse, S. Sustainable Metal Complexes for Organic Light-Emitting Diodes (OLEDs). *Coord. Chem. Rev.* **2018**, *373*, 49–82.

(12) Yersin, H.; Rausch, A. F.; Czerwieniec, R.; Hofbeck, T.; Fischer, T. The Triplet State of Organo-Transition Metal Compounds. Triplet Harvesting and Singlet Harvesting for Efficient OLEDs. *Coord. Chem. Rev.* **2011**, *255*, 2622–2652.

(13) Volz, D.; Wallesch, M.; Fléchon, C.; Danz, M.; Verma, A.; Navarro, J. M.; Zink, D. M.; Bräse, S.; Baumann, T. From Iridium and Platinum to Copper and Carbon: New Avenues for More Sustainability in Organic Light-Emitting Diodes. *Green Chem.* **2015**, *17*, 1988–2011.

(14) Larsen, C. B.; Wenger, O. S. Photoredox Catalysis with Metal Complexes Made From Earth-Abundant Elements. *Chem. Eur. J.* **2017**, *24*, 2039–2058.

(15) Armaroli, N. Photoactive Mono- and Polynuclear Cu(I)–Phenanthrolines. a Viable Alternative to Ru(II)–Polypyridines? *Chem. Soc. Rev.* **2001**, *30*, 113–124.

(16) Mara, M. W.; Fransted, K. A.; Chen, L. X. Interplays of Excited State Structures and Dynamics in Copper(I) Diimine Complexes: Implications and Perspectives. *Coord. Chem. Rev.* **2015**, *282-283*, 2–18.

(17) Mondal, R.; Lozada, I. B.; Davis, R. L.; Williams, J. A. G.; Herbert, D. E. Site-Selective Benzannulation of N-Heterocycles in Bidentate Ligands Leads to Blue-Shifted Emission From $[(P\hat{}N)Cu]_2(M\text{-}X)_2$ Dimers. *Inorg. Chem.* **2018**, *57*, 4966–4978.

(18) Li, G.; Nobuyasu, R. S.; Zhang, B.; Geng, Y.; Yao, B.; Xie, Z.; Zhu, D.; Shan, G.; Che, W.; Yan, L.; Su, Z.; Dias, F. B.; Bryce, M. R. Thermally Activated Delayed

Fluorescence in Cu^{I} Complexes Originating From Restricted Molecular Vibrations. *Chem. Eur. J.* **2017**, *23*, 11761–11766.

(19) Bergmann, L.; Braun, C.; Nieger, M.; Bräse, S. The Coordination- and Photochemistry of Copper(I) Complexes: Variation of N^N Ligands From Imidazole to Tetrazole. *Dalton Trans.* **2018**, *47*, 608–621.

(20) Tsuge, K.; Chishina, Y.; Hashiguchi, H.; Sasaki, Y.; Kato, M.; Ishizaka, S.; Kitamura, N. Luminescent Copper(I) Complexes with Halogenido-Bridged Dimeric Core. *Coord. Chem. Rev.* **2016**, *306*, 636–651.

(21) Perruchas, S.; Le Goff, X. F.; Maron, S.; Maurin, I.; Guillen, F.; Garcia, A.; Gacoin, T.; Boilot, J.-P. Mechanochromic and Thermochromic Luminescence of a Copper Iodide Cluster. *J. Am. Chem. Soc.* **2010**, *132*, 10967–10969.

(22) Gernert, M.; Müller, U.; Haehnel, M.; Pflaum, J.; Steffen, A. A Cyclic Alkyl(Amino)Carbene as Two-Atom π-Chromophore Leading to the First Phosphorescent Linear CuI Complexes. *Chem. Eur. J.* **2017**, *23*, 2206–2216.

(23) Romanov, A. S.; Di, D.; Yang, L.; Fernandez-Cestau, J.; Becker, C. R.; James, C. E.; Zhu, B.; Linnolahti, M.; Credgington, D.; Bochmann, M. Highly Photoluminescent Copper Carbene Complexes Based on Prompt Rather Than Delayed Fluorescence. *Chem. Commun.* **2016**, *52*, 6379–6382.

(24) Shi, S.; Collins, L. R.; Mahon, M. F.; Djurovich, P. I.; Thompson, M. E.; Whittlesey, M. K. Synthesis and Characterization of Phosphorescent Two-Coordinate Copper(I) Complexes Bearing Diamidocarbene Ligands. *Dalton Trans.* **2017**, *46*, 745–752.

(25) Lotito, K. J.; Peters, J. C. Efficient Luminescence From Easily Prepared Three-Coordinate Copper(I) Arylamidophosphines. *Chem. Commun.* **2010**, *46*, 3690–3692.

(26) Hashimoto, M.; Igawa, S.; Yashima, M.; Kawata, I.; Hoshino, M.; Osawa, M. Highly Efficient Green Organic Light-Emitting Diodes Containing Luminescent Three-Coordinate Copper(I) Complexes. *J. Am. Chem. Soc.* **2011**, *133*, 10348–10351.

(27) Krylova, V. A.; Djurovich, P. I.; Aronson, J. W.; Haiges, R.; Whited, M. T.; Thompson, M. E. Structural and Photophysical Studies of Phosphorescent Three-Coordinate Copper(I) Complexes Supported by an N-Heterocyclic Carbene Ligand. *Organometallics* **2012**, *31*, 7983–7993.

(28) Mohankumar, M.; Monti, F.; Holler, M.; Niess, F.; Delavaux-Nicot, B.; Armaroli, N.; Sauvage, J.-P.; Nierengarten, J.-F. Combining Topological and Steric Constraints for the Preparation of Heteroleptic Copper(I) Complexes. *Chem. Eur. J.* **2014**, *20*, 12083–12090.

(29) Leitl, M. J.; Krylova, V. A.; Djurovich, P. I.; Thompson, M. E.; Yersin, H. Phosphorescence Versus Thermally Activated Delayed Fluorescence. Controlling Singlet-Triplet Splitting in Brightly Emitting and Sublimable Cu(I) Compounds. *J. Am. Chem. Soc.* **2014**, *136*, 16032–16038.

(30) Krylova, V. A.; Djurovich, P. I.; Conley, B. L.; Haiges, R.; Whited, M. T.; Williams, T. J.; Thompson, M. E. Control of Emission Colour with N-Heterocyclic Carbene (NHC) Ligands in Phosphorescent Three-Coordinate Cu(I) Complexes. *Chem. Commun.* **2014**, *50*, 7176–7179.

(31) Felder, D.; Nierengarten, J.-F.; Barigelletti, F.; Ventura, B.; Armaroli, N. Highly Luminescent Cu(I)−Phenanthroline Complexes in Rigid Matrix and Temperature Dependence of the Photophysical Properties. *J. Am. Chem. Soc.* **2001**, *123*, 6291–6299.

(32) Czerwieniec, R.; Yu, J.; Yersin, H. Blue-Light Emission of Cu(I) Complexes and Singlet Harvesting. *Inorg. Chem.* **2011**, *50*, 8293–8301.

(33) Nishikawa, M.; Nomoto, K.; Kume, S.; Inoue, K.; Sakai, M.; Fujii, M.; Nishihara, H. Dual Emission Caused by Ring Inversion Isomerization of a 4-Methyl-2-Pyridyl-Pyrimidine Copper(I) Complex. *J. Am. Chem. Soc.* **2010**, *132*, 9579–9581.

(34) Linfoot, C. L.; Leitl, M. J.; Richardson, P.; Rausch, A. F.; Chepelin, O.; White, F. J.; Yersin, H.; Robertson, N. Thermally Activated Delayed Fluorescence (TADF) and Enhancing Photoluminescence Quantum Yields of $[Cu^{I}(Diimine)(Diphosphine)]^{+}$ Complexes-Photophysical, Structural, and Computational Studies. *Inorg. Chem.* **2014**, *53*, 10854–10861.

(35) Gneuß, T.; Leitl, M. J.; Finger, L. H.; Rau, N.; Yersin, H.; Sundermeyer, J. A New Class of Luminescent Cu(I) Complexes with Tripodal Ligands – TADF Emitters for the Yellow to Red Color Range. *Dalton Trans.* **2015**, *44*, 8506–8520.

(36) Czerwieniec, R.; Yersin, H. Diversity of Copper(I) Complexes Showing Thermally Activated Delayed Fluorescence: Basic Photophysical Analysis. *Inorg. Chem.* **2015**, *54*, 4322–4327.

(37) Keller, S.; Prescimone, A.; Bolink, H.; Sessolo, M.; Longo, G.; Martínez-Sarti, L.; Junquera-Hernández, J. M.; Constable, E. C.; Ortí, E.; Housecroft, C. E. Luminescent Copper(I) Complexes with Bisphosphane and Halogen-Substituted 2,2′-Bipyridine Ligands. *Dalton Trans.* **2018**, *124*, 4918–14.

(38) Garakyaraghi, S.; McCusker, C. E.; Khan, S.; Koutnik, P.; Bui, A. T.; Castellano, F. N. Enhancing the Visible-Light Absorption and Excited-State Properties of Cu(I) MLCT Excited States. *Inorg. Chem.* **2018**, *57*, 2296–2307.

(39) McMillin, D. R.; Kirchhoff, J. R.; Goodwin, K. V. Exciplex Quenching of Photo-Excited Copper Complexes. *Coord. Chem. Rev.* **1985**, *64*, 83–92.

(40) Stacy, E. M.; McMillin, D. R. Inorganic Exciplexes Revealed by Temperature-Dependent Quenching Studies. *Inorg. Chem.* **1990**, *29*, 393–396.

(41) Eggleston, M. K.; McMillin, D. R.; Koenig, K. S.; Pallenberg, A. J. Steric Effects in the Ground and Excited States of $Cu(NN)_2$ Systems. *Inorg. Chem.* **1997**, *36*, 172–176.

(42) Christensen, P. R.; Nagle, J. K.; Bhatti, A.; Wolf, M. O. Enhanced Photoluminescence of Sulfur-Bridged Organic Chromophores. *J. Am. Chem. Soc.* **2013**, *135*, 8109–8112.

(43) Cruz, C. D.; Christensen, P. R.; Chronister, E. L.; Casanova, D.; Wolf, M. O.; Bardeen, C. J. Sulfur-Bridged Terthiophene Dimers: How Sulfur Oxidation State Controls Interchromophore Electronic Coupling. *J. Am. Chem. Soc.* **2015**, *137*, 12552–12564.

(44) Brown, C. M.; Kitt, M. J.; Xu, Z.; Hean, D.; Ezhova, M. B.; Wolf, M. O. Tunable Emission of Iridium(III) Complexes Bearing Sulfur-Bridged Dipyridyl Ligands. *Inorg. Chem.* **2017**, *56*, 15110–15118.

(45) Brown, C. M.; Carta, V.; Wolf, M. O. Thermochromic Solid-State Emission of Dipyridyl Sulfoxide Cu(I) Complexes. *Chem. Mater.* **2018**, *30*, 5786–5795.

(46) Caron, E.; Brown, C. M.; Hean, D.; Wolf, M. O. Variable Oxidation State Sulfur-Bridged Bithiazole Ligands Tune the Electronic Properties of Ruthenium(II) and Copper(I) Complexes. *Dalton Trans.* **2019**, *48*, 1263–1274.

(47) Cuttell, D. G.; Kuang, S.-M.; Fanwick, P. E.; McMillin, D. R.; Walton, R. A. Simple Cu(I) Complexes with Unprecedented Excited-State Lifetimes. *J. Am. Chem. Soc.* **2002**, *124*, 6–7.

(48) Zhang, L.; Bin Li. Room-Temperature Pure Blue-Emitting Phosphorescent Multinuclear Cu(I)-Based Emitters. *J. Electrochem. Soc.* **2009**, *156*, J174.

(49) Hong, M.-W.; Song, L.; Zhao, Y.; Qin, L.-S.; Wang, C.-Y.; Shi, H.-S.; Guo, J.-Y.; Tao, X.-D.; Shu, K.-Y.; Chai, W.-X. Synthesis and Characterizations of Strongly Phosphorescent Copper(I) Halide Complexes with Bridged Bis[2-(Diphenylphosphino)Phenyl]Ether Ligand. *J. Clust. Sci.* **2014**, *25*, 1627–1640.

(50) Kaeser, A.; Mohankumar, M.; Mohanraj, J.; Monti, F.; Holler, M.; Cid, J.-J.; Moudam, O.; Nierengarten, I.; Karmazin-Brelot, L.; Duhayon, C.; et al. Heteroleptic Copper(I) Complexes Prepared From Phenanthroline and Bis-Phosphine Ligands. *Inorg. Chem.* **2013**, *52*, 12140–12151.

(51) Moudam, O.; Kaeser, A.; Delavaux-Nicot, B.; Duhayon, C.; Holler, M.; Accorsi, G.; Armaroli, N.; Séguy, I.; Navarro, J.; Destruel, P.; et al. Electrophosphorescent Homo- and Heteroleptic Copper(I) Complexes Prepared From Various Bis-Phosphine Ligands. *Chem. Commun.* **2007**, *29*, 3077–3079.

(52) Qin, L.; Zhang, Q.; Sun, W.; Wang, J.; Lu, C.; Cheng, Y.; Wang, L. Novel Luminescent Iminephosphine Complex of Copper(I) with High Photochemical and Electrochemical Stability. *Dalton Trans.* **2009**, *280*, 9388–4.

(53) Kaeser, A.; Moudam, O.; Accorsi, G.; Séguy, I.; Navarro, J.; Belbakra, A.; Duhayon, C.; Armaroli, N.; Delavaux-Nicot, B.; Nierengarten, J.-F. Homoleptic Copper(I), Silver(I), and Gold(I) Bisphosphine Complexes. *Eur. J. Inorg. Chem.* **2014**, *2014*, 1345–1355.

(54) Addison, A. W.; Sinn, E. A Stable Bis(Thiolate) of Copper(II) with Long Axial Copper-Sulfur Linkages: Crystal and Molecular Structure of Trans-[Cu(Cyclam)(SC_6F_5)$_2$]. *Inorg. Chem.* **1983**, *22*, 1225–1228.

(55) Andrés-Tomé, I.; Fyson, J.; Dias, F. B.; Monkman, A. P.; Iacobellis, G.; Coppo, P. Copper(I) Complexes with Bipyridyl and Phosphine Ligands: a Systematic Study. *Dalton Trans.* **2012**, *41*, 8669–8674.

(56) Connelly, N. G.; Geiger, W. E. Chemical Redox Agents for Organometallic Chemistry. *Chem. Rev.* **1996**, *96*, 877–910.

(57) Cardona, C. M.; Li, W.; Kaifer, A. E.; Stockdale, D.; Bazan, G. C. Electrochemical Considerations for Determining Absolute Frontier Orbital Energy Levels of Conjugated Polymers for Solar Cell Applications. *Adv. Mater.* **2011**, *23*, 2367–2371.

(58) Miller, M. T.; Gantzel, P. K.; Karpishin, T. B. Effects of Sterics and Electronic Delocalization on the Photophysical, Structural, and Electrochemical Properties of 2,9-Disubstituted 1,10-Phenanthroline Copper(I) Complexes. *Inorg. Chem.* **1999**, *38*, 3414–3422.

(59) Yang, L.; Feng, J.-K.; Ren, A.-M.; Zhang, M.; Ma, Y.-G.; Liu, X.-D. Structures, Electronic States and Electroluminescent Properties of a Series of Cu^{I} Complexes. *Eur. J. Inorg. Chem.* **2005**, *2005*, 1867–1879.

(60) Zhang, Y.; Schulz, M.; Wächtler, M.; Karnahl, M.; Dietzek, B. Heteroleptic Diimine–Diphosphine Cu(I) Complexes as an Alternative Towards Noble-Metal Based Photosensitizers: Design Strategies, Photophysical Properties and Perspective Applications. *Coord. Chem. Rev.* **2018**, *356*, 127–146.

(61) Garakyaraghi, S.; Danilov, E. O.; McCusker, C. E.; Castellano, F. N. Transient Absorption Dynamics of Sterically Congested Cu(I) MLCT Excited States. *J. Phys. Chem. A* **2015**, *119*, 3181–3193.

(62) Cuttell, D. G.; Kuang, S.-M.; Fanwick, P. E.; McMillin, D. R.; Walton, R. A. Simple Cu(I) Complexes with Unprecedented Excited-State Lifetimes. *J. Am. Chem. Soc.* **2002**, *12*, 6–7.

(63) Parker, C. A.; Hatchard, C. G. Triplet-Singlet Emission in Fluid Solution. *J. Phys. Chem.* **1962**, *66*, 2506–2511.

(64) Bergmann, L.; Hedley, G. J.; Baumann, T.; Bräse, S.; Samuel, I. D. W. Direct Observation of Intersystem Crossing in a Thermally Activated Delayed Fluorescence Copper Complex in the Solid State. *Sci. Adv.* **2016**, *2*, e1500889.

(65) Vandromme, L.; Reißig, H.-U.; Gröper, S.; Rabe, J. P. Practical Routes to 2,6-Disubstituted Pyridine Derivatives. *European Journal of Organic Chemistry* **2008**, *2008*, 2049–2055.

(66) Bruker, S. *Version 6.02 (Includes XPREP and SADABS)*; Bruker AXS Inc., 1999.

(67) Palatinus, L.; Chapuis, G. SUPERFLIP– a Computer Program for the Solution of Crystal Structures by Charge Flipping in Arbitrary Dimensions. *J. Appl. Crystallogr.* **2007**, *40*, 786–790.

(68) Betteridge, P. W.; Carruthers, J. R.; Cooper, R. I.; Prout, K.; Watkin, D. J. CRYSTALS Version 12: Software for Guided Crystal Structure Analysis. *J. Appl. Crystallogr.* **2003**, *36*, 1487–1487.

(69) Cooper, R. I.; Thompson, A. L.; Watkin, D. J. CRYSTALS Enhancements: Dealing with Hydrogen Atoms in Refinement. *J. Appl. Crystallogr.* **2010**, *43*, 1100–1107.

(70) Lee, C.; Yang, W.; Parr, R. G. Development of the Colle-Salvetti Correlation-Energy Formula Into a Functional of the Electron Density. *Phys. Rev. B* **1988**, *37*, 785–789.

(71) Becke, A. D. Density-Functional Thermochemistry. III. the Role of Exact Exchange. *J. Chem. Phys.* **1993**, *98*, 5648–5652.

(72) Stephens, P. J.; Devlin, F. J.; Chabalowski, C. F.; Frisch, M. J. Ab Initio Calculation of Vibrational Absorption and Circular Dichroism Spectra Using Density Functional Force Fields. *J. Phys. Chem.* **1994**, *98*, 11623–11627.

(73) Hay, P. J.; Wadt, W. R. Ab Initioeffective Core Potentials for Molecular Calculations. Potentials for K to Au Including the Outermost Core Orbitals. *J. Chem. Phys.* **1985**, *82*, 299–310.

(74) Jamorski, C.; Casida, M. E.; Salahub, D. R. Dynamic Polarizabilities and Excitation Spectra From a Molecular Implementation of Time-Dependent Density-Functional Response Theory: N_2 as a Case Study. *J. Chem. Phys.* **1996**, *104*, 5134–5147.

(75) Casida, M. E.; Jamorski, C.; Casida, K. C.; Salahub, D. R. Molecular Excitation Energies to High-Lying Bound States From Time-Dependent Density-Functional Response Theory: Characterization and Correction of the Time-Dependent Local Density Approximation Ionization Threshold. *J. Chem. Phys.* **1998**, *108*, 4439–4449.

(76) Petersilka, M.; Gossmann, U.; Gross, E. Excitation Energies From Time-Dependent Density-Functional Theory. *Phys. Rev. Lett.* **1996**, *76*, 1212–1215.

(77) Grimme, S.; Antony, J.; Ehrlich, S.; Krieg, H. A Consistent and Accurate Ab Initio Parametrization of Density Functional Dispersion Correction (DFT-D) for the 94 Elements H-Pu. *J. Chem. Phys.* **2010**, *132*, 154104.

Table of Contents Synopsis and Graphic

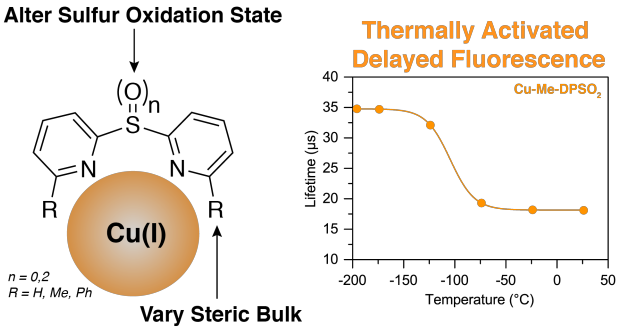

Heteroleptic Cu(I) complexes bearing sulfur-bridged dipyridyl ligands are shown to exhibit thermally activated delayed fluorescence (TADF). Through a combination of altering oxidation state at the sulfur (S or SO_2) and substitution at the dipyridyl ligands, mono- or bimetallic species are isolated. Higher sulfur oxidation state (SO_2) results in a red-shift of emission in the solid state.